ANALYTICAL BIOCHEMISTRY **249,** 94–102 (1997)
ARTICLE NO. AB972160

Label-Free Monitoring of DNA–Ligand Interactions

Jacob Piehler,*[,1] Andreas Brecht,* Günter Gauglitz,* Marion Zerlin,†
Corinna Maul,‡ Ralf Thiericke,‡ and Susanne Grabley‡

**Institut für Physikalische Chemie, Auf der Morgenstelle 8, D-72076 Tübingen, Germany; †Molekulare Zellbiologie, Max-Planck-Gesellschaft, Drackendorfstrasse 1, D-07745 Jena, Germany; and ‡Hans-Knöll-Institut für Naturstoff-Forschung e.V., Beutenbergstrasse 11, D-07745 Jena, Germany*

Received December 3, 1996

We report on the label- and isotope-free monitoring of DNA interactions with low-molecular-weight ligands. An optical technique based on interference at thin layers was used to monitor in real time binding of ligands at DNA which was immobilized by Coulomb interactions at a positively charged surface. Approximately 2 ng DNA/mm^2 was irreversibly bound to the surface, which remained stable over several days. This result was confirmed by characterization of the layer using spectroscopic ellipsometry. During incubation of immobilized DNA with a variety of intercalators and other DNA-binding compounds in a flow system, interactions were monitored by reflectometric interference spectroscopy. Binding effects between 10 and 400 pg/mm^2 were detected unambiguously. Nonspecific binding effects were excluded by using a negatively charged reference surface. Variation of intercalator concentration allowed the characterization of interaction with respect to kinetics and thermodynamics by the evaluation of binding rate and equilibrium coverage. The affinity constants were determined in the range between 10^5 and 10^6 M^{-1}, in good agreement to those obtained by homogeneous phase assays. Association rate constants between 10^3 and 10^5 $M^{-1}s^{-1}$ and dissociation rate constants between 10^{-1} and 10^{-2} s^{-1} were determined by evaluation of the binding curves. Both the fast and simple test format and a universal applicability make the new technique described attractive for detecting and characterizing interaction of low-molecular-weight molecules with DNA.

A number of natural products and synthetic compounds are capable of forming complexes with DNA (1). It has been demonstrated that DNA-binding agents possess, e.g., anti-tumor, anti-viral, or anti-microbial activity, and certain substances are of pharmacological and medical importance (2). Many anti-tumor drugs exert their action by interfering with the function of DNA. Modes of interaction include noncovalent binding such as intercalation and groove binding (1), drug–DNA adduct formation, e.g., by cisplatin covalent binding (3), and DNA backbone scission, e.g., by bleomycin or enediyne antibiotics (4, 5). Anthracycline antibiotics constitute an important family of intercalative anti-tumor drugs and some of them, e.g., doxorubicin (6), have been used clinically as components in chemotherapeutic treatments of different kinds of cancer. Intercalators bind to DNA by inserting their planar chromophores between adjacent DNA base pairs. Frequently, these complexes are further stabilized by hydrogen bond formation between the DNA bases and the sugar moieties appended to the aglycon. Typically, association constants in the range of $5 \cdot 10^5$–$5 \cdot 10^6$ M^{-1} are observed for this interaction principle.

The interaction of low-molecular-weight compounds with nucleic acids is subject of numerous biophysical and biochemical investigations. Several methods are based on the detection of a change in absorbance, fluorescence or circular dichroism of the ligand during binding to DNA (1). Some short-term procedures have been designed which are applicable for ligand screening: (i) bacterial colorimetric test methods based on the induction by DNA binding agents of the SOS function (7); (ii) displacement assays based on spectroscopic detection of ethidium bromide or other intercalators (8, 9); and (iii) detection of an inhibition of the polymerase chain reaction (10). DNA-intercalating drugs are frequently detected by an increase of the melting temperature of DNA (11) as they increase the stability of the interstrand binding of double-stranded DNA. However, these effects are based on distinct properties of the ligand or the interaction mechanisms. Therefore, all these techniques are not suitable for investigations of ligand–DNA interactions in general.

[1] To whom correspondence should be addressed. Fax: 49(0)7071 29 74667. E-mail: jacob.piehler@uni-tuebingen.de.

0003-2697/97 $25.00

In recent years, a range of techniques for the label-free and real time monitoring of biochemical interactions by using solid phases have found increasing attention. These methods allow monitoring of binding events at solid–liquid interfaces and therefore access to both kinetic and thermodynamic parameters of the interaction (13). All these techniques are based on monitoring of parameters which relate to the amount of biological material deposited at a transducer surface. Most methods for the label-free detection of binding reactions, in particular commercially available techniques, make use of optical detection systems which are based on the fact that the refractive index of organic material is higher than the value found for aqueous media ($n_D \approx 1.333$). Thus, the coating of biological material at a surface will either lead to a local increase of the refractive index or to the formation of an adlayer optically distinct from the surrounding solution. A wide range of techniques have been investigated during the last decade (e.g., Refs. (14–17)). The limits of detection reported are in the range of a few pg/mm^2, which corresponds to less than 1‰ of a typical protein monolayer.

Direct detection of low-molecular-weight ligands binding to an immobilized receptor appears to be difficult because the surface loading by a monolayer coverage is about one dimension below the values found for proteins. In general, the binding effect becomes even smaller due to the limited density of binding sites provided by the immobilized macromolecular receptor compound. The overall binding effects at the point of saturation may be in the range of a few tens of pg/mm^2. Therefore, competitive assays with an immobilized derivative are preferred for detection of receptor interactions with low-molecular-weight ligands (18). For direct studies of these interactions, high performance of the monitoring device is required. So far, this has been demonstrated only by a few systems (19, 20). The detection of low-molecular-weight compounds binding to immobilized receptors requires two main assumptions: a high sensitivity detection system and an effective way to immobilize intact receptors with a high density.

In this paper we report on the application of a new highly sensitive label-free detection technique in order to monitor low-molecular-weight compounds binding to immobilized DNA. Reflectometric interference spectroscopy (RIfS)[2] is applied for monitoring of the binding events. Reproducible and efficient immobilization of the DNA by a simple, noncovalent adsorption procedure is presented. Binding of intercalators (Fig. 1) and various metabolites to the adsorbed DNA is investigated and compared with results derived from DNA-melting studies. Thermodynamic and kinetic parameters of the intercalator binding are obtained from evaluation of the binding curves at various concentrations.

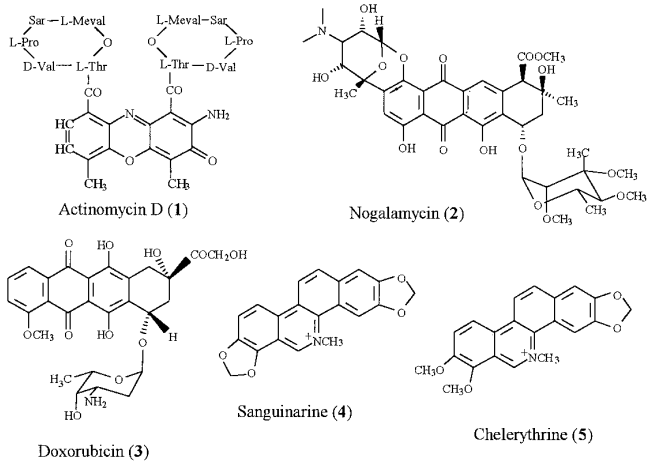

FIG. 1. Structures of the intercalators investigated.

MATERIALS AND METHODS

Chemicals and Biochemicals

Branched polyethyleneimine (PEI, 50.000 g/mol), salmon sperm DNA, chelerythrine **(5)**, and nogalamycin **(2)** were purchased from Sigma (Deisenhofen, Germany). Actinomycin D **(1)**, doxorubicin **(3)**, sanguinarine **(4)**, and iodeosin were purchased from Fluka (Neu-Ulm, Germany) and polyvinyl sulfate (PVS, 50,000 g/mol) was from Aldrich (Steinheim, Germany).

Sheared DNA was obtained by sonication (Labsonic U; B. Braun, Melsungen, Germany) of salmon sperm DNA in solution (2 mg/ml) for 6 min. A DNA strand length of 300–3000 bp was determined by agarose gel electrophoresis.

Melting Curves

DNA melting curve measurements were carried out with a Cary 1 Bio UV/VIS spectrophotometer (Varian, Darmstadt, Germany). All substances were dissolved in methanol at a concentration of 1 mg/ml. Ten microliters of this solution was added to a mixture of 400 μl sodium chloride solution (50 or 100 mM) and 10 μl of sonified DNA solution (1 mg/ml) (Fig. 1).

RIFS Technique and Setup

Binding events were monitored by use of RIfS. This technique is based on the spectral distribution of reflectance from transparent thin layers. The partial beams reflected from each surface of the film interfere and produce a distinct spectral reflectance pattern with alternating maxima and minima of reflectance due to constructive and destructive interference of the re-

[2] Abbreviations used: RIfS, reflectometric interference spectroscopy; PEI, polyethyleneimine; PVS, polyvinyl sulfate; PBS, phosphate-buffered saline; CVD, chemical vapor deposition.

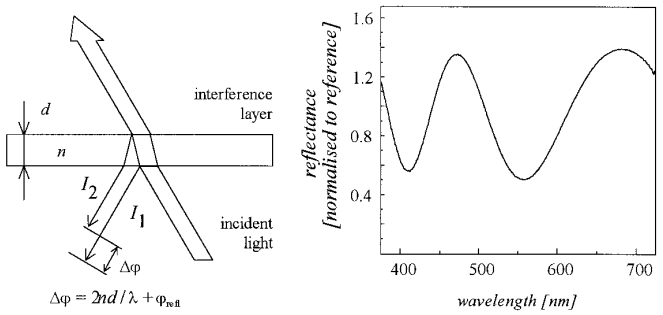

FIG. 2. Principle of the detection of affinity interactions by RIfS (n and d are the refractive index and the thickness of the layer, I_1 and I_2 are the intensities of the reflected light beams, $\Delta\phi$ is the difference in the optical path length of the two beams, and ϕ_{refl} is the phase shift upon reflection).

flected radiation (Fig. 2). From this pattern the thickness of a film can be quantified. Biological material deposited at the surface during a binding event increases the optical thickness of the interference layer, leading to a shift in the interference pattern.

First attempts to use the interference colors from thin films for the monitoring of bioaffinity reactions were reported in 1939 by Langmuir and Schaefer (21). In recent years we have improved this technique to allow on-line monitoring of binding reactions with high resolution (17). The capability of this transducer for the detection of low-molecular-weight compounds binding to an immobilized receptor was demonstrated recently (20). The experimental setup for detection of affinity interactions (Fig. 3) has already been published in detail before (22): white light from a tungsten light source is guided to the transducer using bifurcated fiber optics (PMMA; Microparts, Dortmund, Germany). The reflected light is collected by the same fiber and spectrally detected by a diode array spectrometer (MCS 410, 512 diodes, 16 bit nominal resolution; Carl Zeiss, Jena, Germany). The transducer is mounted in a flow cell and sample handling is carried out by flow injection analysis using an ASIA system from Ismatec (Zürich, Switzerland), including an autosampler module. Data acquisition and evaluation as well as sample handling control was carried out with a PC.

The binding curves were recorded as apparent optical thickness nd vs time. The optical thickness was determined from the interference spectrum by polynomial regression of a part of the curve as described in (17). A change in optical thickness Δnd of 1 pm rms corresponds to approximately 1 pg/mm^2 of biological material (23).

Surface Modification

Interference layers (10 nm Ta_2O_5 and 500 nm SiO_2 on float glass) were manufactured by Schott (Mainz, Germany) using a plasma-impulse CVD process. Prior to use, the layers were cleaned in a freshly prepared mixture of 60% H_2SO_4 and 40% H_2O_2. This procedure results in a highly hydrophilic (contact angle 0°) and acidic surface. All further steps were carried out in the flow system, and the binding effects were monitored by RIfS. To promote noncovalent adsorption of DNA at the transducer surface, in a first step a layer of PEI was adsorbed to the surface. PEI was incubated in a concentration of 100 μg/ml in PBS, pH 7.4, for 80 s. After rinsing with PBS, the resulting cationic surface was loaded with DNA by incubation with a solution of 100 μg/ml in PBS for 200 s. Afterward, the flow cell was again rinsed with PBS. For the investigation of nonspecific binding effects due to the polyanionic properties of the DNA, the interactions of the substances with an immobilized negatively charged polymer were investigated. This reference surface was prepared by incubation of a solution of polyvinyl sulfate at the PEI-pretreated surface as described for DNA.

The DNA/PEI bilayer system was characterized by spectroscopic ellipsometry using an ES4G spectral ellipsometer (Sopra, Paris, France). The immobilization procedure was carried out on oxidized silicon wafers (170 nm SiO_2; Wacker, Burghausen, Germany). The measurements were carried out in buffer solution using an incident angle of 70°C and a spectral range from 300 to 800 nm with a resolution of 2 nm. The experimental details for the investigation of thin biochemical layers are published elsewhere (24).

Binding Assays and Data Analysis

Binding of various ligands was investigated at a concentration of 10 μg/ml and a flow rate of 100 μl/min.

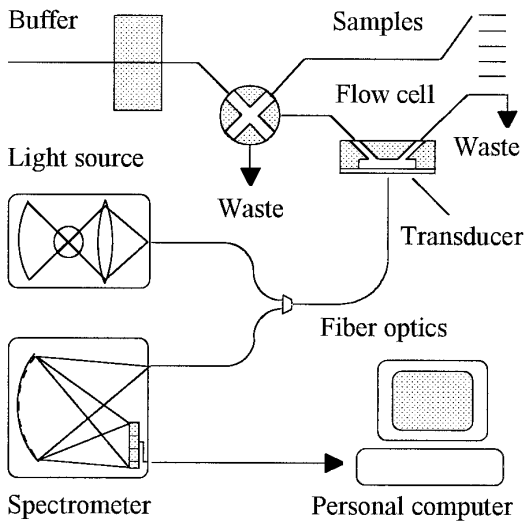

FIG. 3. Experimental setup used for monitoring binding events.

After recording of a prerun baseline for 120 s, the ligands were injected and incubated for 180 s. During rinsing of the flow cell with fresh buffer, dissociation was monitored for a time interval of 560 s. Spectra were recorded at a frequency of 0.2 Hz. For further evaluation of the binding curves, the baseline was corrected by subtraction of the prerun layer thickness.

Thermodynamics and kinetics of intercalator binding at immobilized DNA were investigated by monitoring binding curves at various intercalator concentrations using the same protocol as that described above. Adsorption isotherms were obtained by plotting the equilibrium change in optical thickness Δnd reached during the binding event vs the intercalator concentration c. Further information about the interaction was derived by plotting $\Delta nd/c$ vs Δnd (Scatchard plot, cf. Ref. (25)). The affinity constant K was determined from the slope of this curve and the maximum coverage of the binding sites Γ_{max} was estimated from the abscissa intercept.

Binding kinetics were investigated by evaluation of the association and dissociation part of the binding curves. Various methods for the kinetic analysis of binding curves have been discussed (26, 27). Frequently, both the association rate k_a and dissociation rate k_d constant are derived by fitting of a model to the binding curves (27). The surface coverage Γ as a function of time is given by

$$\Gamma = \Gamma_0 \cdot (1 - e^{-(k_a \cdot c + k_d) \cdot t}), \qquad [1]$$

assuming pseudo-first-order association kinetics and first-order dissociation kinetics (28). More complex binding events are better modeled by a biexponential curve of the same type (29). These models were fitted to the binding curves using a non-linear least squares algorithm (software ORIGIN from MicroCal, Northampton, MA). In all cases, the single exponential model was fitted in the first step. The parameters of the second exponential term were fitted in a following step if systematic differences between the model and the binding curve were significant.

The exponential time constants k_s were plotted vs the intercalator concentrations. The association rate constant was determined from the slope of this curve. The dissociation rate constant was estimated from the intercept. More reliable values for the dissociation rate constant were obtained by fitting an exponential decay to the dissociation part of the binding curve. The affinity constant K was derived from the ratio of association and dissociation rate constants

$$K = \frac{k_a}{k_d}. \qquad [2]$$

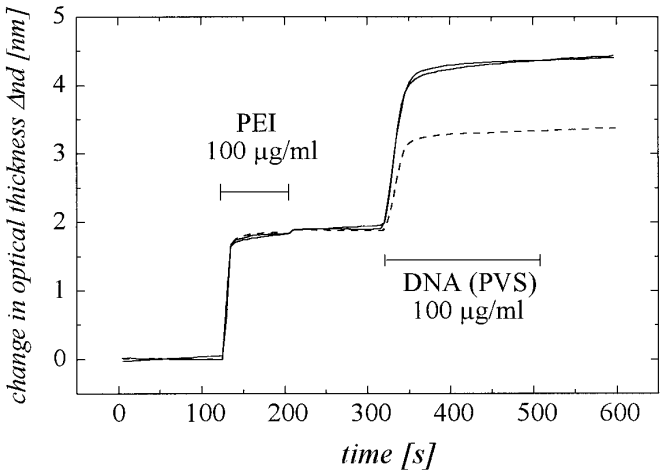

FIG. 4. Immobilization of DNA (—) and PVS (· · ·) after pretreatment of the surface with PEI.

RESULTS AND DISCUSSION

System Performance

Binding events were monitored by reflectometric interference spectroscopy. The performance of the detection system was estimated from the noise of the baseline. A typical baseline interval (200 s) was fitted by linear regression (data not shown). The standard deviation of the residuals from the fit was taken as an estimate for the rms noise of the thickness determination and found to be 0.8 pm. As a signal of 1 nm corresponds to a surface loading of about 1 ng/mm^2, changes in surface loading of less than 3 pg/mm^2 can be resolved by the RIfS technique. A low drift of the signal of less than 0.005 pm/s demonstrates the high stability of this simple setup.

DNA Immobilization

During incubation with PEI, a change in optical thickness of 1.5–1.8 nm was observed (Fig. 4, first step). The curve indicates rapid binding of the polycation to the surface. The maximum binding effect was reached within 20 s. The layer remained stable during subsequent washing with PBS. Incubation of the resulting surface with DNA (Fig. 4) resulted in an increase in optical thickness of 2.2 ± 0.2 nm ($N = 5$). The binding kinetics was slower compared to the binding of the PEI, which is probably due to mass transport limitations. A surface loading by DNA of approximately 2 ng/mm^2 is estimated from this response, which corresponds to $2 \cdot 10^{12}$ base pairs (bp) per mm^2 (assuming a molecular mass of 600 g/bp). During rinsing with PBS no significant decrease of the surface loading was observed, indicating a stable attachment of the DNA at the surface.

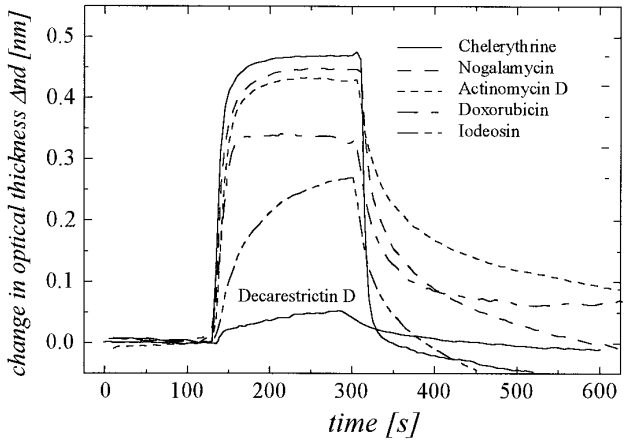

FIG. 5. Sensor response during incubation of various intercalators and other compounds at a concentration of 10 μg/ml.

The binding of polyvinyl sulfate as a reference compound showed similar behavior. A stable increase in optical thickness of 1.2 nm was found (Fig. 4, dotted line). This lower loading compared to the DNA is probably due to the lower molecular mass per charged group of this polymer.

By spectroscopic ellipsometry, a layer thickness of 4.5 nm DNA was found, assuming a refractive index of $n_D = 1.4$. From these parameters, a surface loading of 2 ng/mm^2 DNA was determined, in good agreement to the results obtained by RIfS.

Interactions with Immobilized DNA

The interaction of various intercalators and metabolites with the immobilized DNA at a concentration of 10 μg/ml is shown in Fig. 5. The association of DNA and the substances was reversible, although in some cases the initial baseline was not reached. The intercalators (chelerythrine **(5)**, nogalamycin **(2)**, actinomycin D **(1)**, and doxorubicin **(3)**) showed a high increase of the optical thickness. The equilibrium response observed at 10 μg/ml correspond to surface loadings of approximately 350–400 pg/mm^2 or $2–5 \cdot 10^{11}$ molecules/mm^2, respectively. Assuming a surface concentration of $2 \cdot 10^{12}$ binding sites per mm^2 from the DNA loading, an occupation by the intercalators between 10 and 20% can be estimated from these signals. Interestingly, the binding behavior of the dye iodeosin, which is structurally related to the intercalators, is different. It shows a strong interaction with the DNA with a lower association and dissociation rate. This effect is probably due to a different binding mechanism. At the polyanionic reference layer, no significant binding of these compounds was observed. This experiment proves that the binding effects detected during incubation of the intercalators at the immobilized DNA were exclusively due to specific interactions.

The binding effects of the weak-binding metabolites are one dimension below the effects observed for the intercalators, but still fast binding kinetics are observed. This indicates either lower affinity constants or lower recruitment of DNA binding sites. Unambiguously, a minimum binding effect of 10 pm was detected for the weakest-binding compound tested. This corresponds to a surface concentration of approximately $1 \cdot 10^{10}$ molecules/mm^2 and a stoichiometry of 1 molecule bound per 200 base pairs (120,000 g/mol) of the DNA strand. Details of the experiments about the weak-binding compounds tested will be the subject of an forthcoming paper.

The results were well confirmed by the DNA melting curves measured: The strong-binding compounds alter the melting point of DNA in a range of 9–11°C. In contrast, weak-binding compounds induce temperature shifts in the range of 0.7–0.8°C. An overview about the binding effects at immobilized DNA found in this study is given in Table 1.

Biomolecular Interaction Analysis

Monitoring the binding event at different ligand concentrations allowed kinetic and thermodynamic characterization of the interaction process in detail. These studies were carried out with four intercalators (com-

TABLE 1

Comparison of Sensor Response and Shift of DNA Melting Point for Various Intercalators

No.	Compound	Molecular mass [g/mol]	Shift of DNA melting point	Sensor response (RIfS)	Binding to PVS (RIfS)
1	Actinomycin D (**1**)	1255.4	8.8	+++	0
2	Nogalamycin (**2**)	787.8	10.8	+++	0
3	Doxorubicin (**3**)	543.3	11.1	+++	0
4	Sanguinarine (**4**)	331.8	9.7	+++	0
5	Chelerythrine (**5**)	348.2	n.d.	+++	0
6	Iodeosin	879.9	0.7	++	0
7	Decarestrictin D (30)	186.1	0.8	+	0

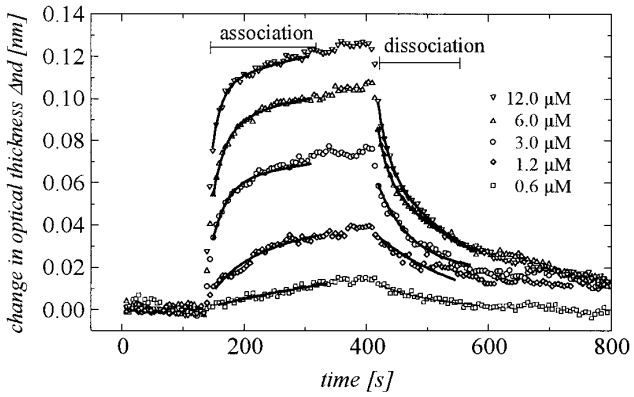

FIG. 6. Binding of actinomycin D **(1)** at various concentrations to immobilized DNA and fit of the kinetic model functions for association and dissociation (—).

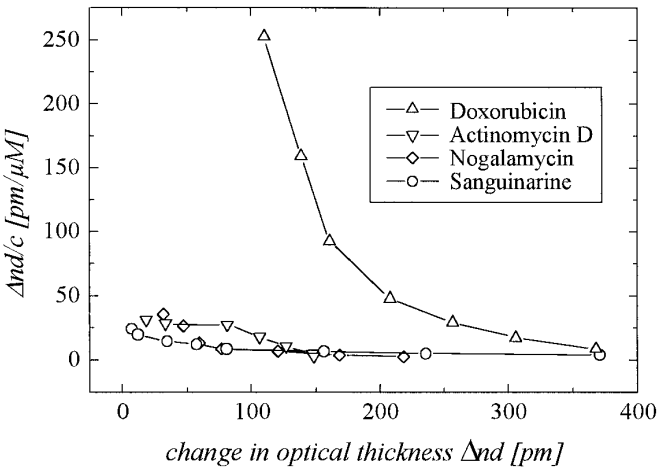

FIG. 8. Scatchard plots for binding of the intercalators to immobilized DNA.

pounds 1–4) by recording binding curves at concentrations between 0.5 and 100 μM. Typical binding curves of the intercalator actinomycin D **(1)** at various concentrations are shown in Fig. 6. The thermodynamic approach for the assessment of affinity constants is the analysis of the equilibrium coverage. Quantification was possible due to the reversible binding and fast association and dissociation kinetics observed for the intercalators. Binding isotherms obtained from the equilibrium signal are shown in Fig. 7 for the intercalators investigated. For all intercalators, an increase of the equilibrium coverage with increasing concentrations was observed at low concentrations ($<$10 μM). At higher concentrations ($>$25 μM), the intercalators showed different behavior: for actinomycin D **(1)**, no further increase of the equilibrium coverage was observed, indicating maximum occupation of the binding sites. The equilibrium coverage of the other intercalators further increased at concentrations above 25 μM, in particular for sanguinarine **(4)** and nogalamycin **(2)**.

The affinity constants of the interaction were determined from Scatchard plots shown in Fig. 8. Again, significant differences between the intercalators were observed. For doxorubicin **(3)** a much higher slope of the curve was observed than for the other intercalators. An enlargement of the Scatchard plot showing the other three intercalators in detail is presented in Fig. 9. A linear correlation in the concentration range investigated was found for actinomycin D **(1)**. Significant deviations from linearity were observed for nogalamycin **(2)**, sanguinarine **(4)**, and doxorubicin **(3)**. This observation is in agreement with results from homogeneous phase assays (32). Investigations on the deviation from linearity of the Scatchard plot of nogalamycin **(2)** have indicated that different binding mechanisms

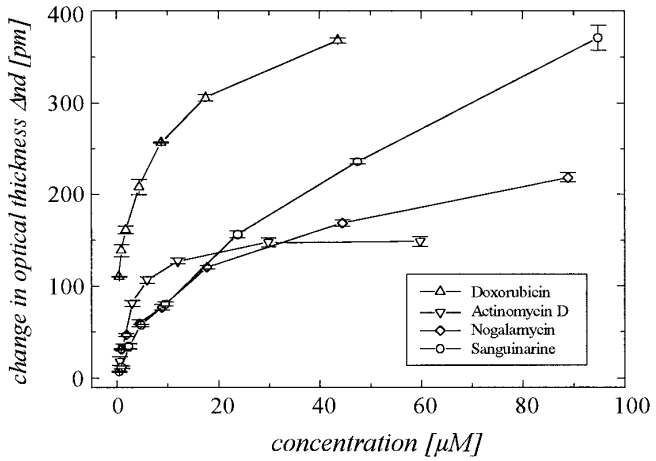

FIG. 7. Adsorption isotherms for intercalator binding to immobilized DNA.

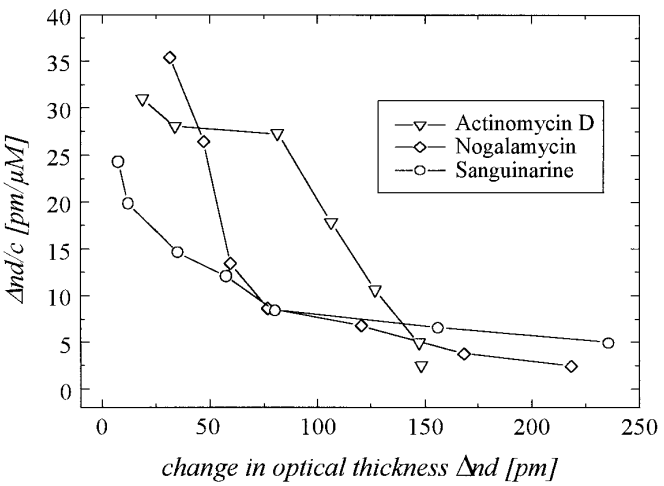

FIG. 9. Enlargement of the Scatchard plots shown in Fig. 8.

TABLE 2

Results from Biomolecular Interaction Analysis: Affinity Constants K Obtained from Scatchard Plots, Binding Site Concentration n, Association Rate Constants k_a, Dissociation Rate Constants k_d, and Affinity Constants K Obtained from Kinetic Analysis of the Binding Curve

Intercalator	Equilibrium coverage (K/liters/mol))	n	Kinetic analysis			Literature (K (liters/mol))
			k_a (liters/mol/s)	k_d (s^{-1})	K (liters/mol)	
Actinomycin D (**1**)	$(3 \pm 0.3)\cdot 10^5$	4%	$(6 \pm 1)\cdot 10^3$	0.02 ± 0.005	$3\cdot 10^5$	$3\cdot 10^6$ (31)
Doxorubicin (**3**)	$(6 \pm 2)\cdot 10^6$	10%	$>10^5$	0.05 ± 0.01	Approx. $2\cdot 10^6$	$3\cdot 10^6$ (6)
Nogalamycin (**2**)	$(7.8 \pm 0.3)\cdot 10^5$	3%	$(4 \pm 0.5)\cdot 10^4$	0.04 ± 0.006	$1\cdot 10^6$	$2\cdot 10^6$ (32)
Sanguinarine (**4**)	$(3 \pm 1)\cdot 10^5$	4%	Approx. 10^5	0.2 ± 0.04	Approx. $5\cdot 10^5$	$9.5\cdot 10^5$ (33)

Note. Reference data for the affinity constants K determined by homogeneous phase assays are given in the last column.

are possible (32, 34): (i) Strong intercalative binding between the base pairs and (ii) weak binding on the external surface of DNA. These two interaction mechanisms explain the nonlinearity due to a higher and a lower affinity constant. In these cases, the affinity constant of the stronger interaction was determined by evaluation of the Scatchard plot at low responses, i.e., the steepest part of the curve.

The results are summarized in Table 2 and compared with reference data from literature (6, 30–32). In principle, the results determined by this method correspond well to the data found by homogeneous phase assays. However, some deviations could be explained by different experimental conditions. In particular the salt concentration strongly affects the intercalation process and causes a change in the observed affinity constant. Loss of material in the sample handling system due to adsorption of the hydrophobic intercalators at the tubing probably leads to a lower effective concentration, in particular at low sample concentrations. This effect could also explain the weak discrepancies to literature data.

The maximum coverage of the strong, intercalative binding sites Γ_{max} was estimated from the intercept at the abscissa of the Scatchard plots. The fraction of base pairs n available for intercalation can be determined by comparison with the total DNA loading Γ_{DNA}

$$n = \frac{\Gamma_{max}\cdot MW_{bp}}{\Gamma_{DNA}\cdot MW_{int}}, \qquad [3]$$

taking the molecular mass of the intercalator MW_{int} and the molecular mass per base pair MW_{bp} into account. This fraction was found to be approximately 3% for nogalamycin **(2)**, 4% for sanguinarine **(4)** and actinomycin D **(1)**, and 9% for doxorubicin **(3)**. Homogeneous phase assays show that approximately 10–15% of the base pairs are available for intercalation, indicating that several binding sites are not accessible which is probably due to the immobilization of the DNA.

A particular advantage of direct monitoring of the binding event is the possibility for investigation of the binding kinetics. The binding curves were evaluated by fitting Eq. [1], assuming pseudo-first-order kinetics for the DNA–intercalator interaction as shown in Fig. 6 for actinomycin D **(1)**. Binding curves at higher intercalator concentrations (>10 μM) did not show simple exponential behavior. Reasonably, this effect can be explained by the different modes of strong and weak interaction of the intercalators with DNA. In these cases, a second exponential term was added to the model function. The exponential time constant k_s of the faster binding process (i.e., strong, intercalative) was plotted versus the intercalator concentration as shown in Fig. 10 for actinomycin D **(1)**. An association rate constant k_a of 6000 ± 1000 liters/mol/s from the slope of the curve and a dissociation rate constant k_d of 0.02 s^{-1} from the intercept were obtained for this intercalator. Accurate determination of the association rate constants was not possible for all intercalators because the binding process was too rapid. Sample handling appeared to be the limiting parameter for the time reso-

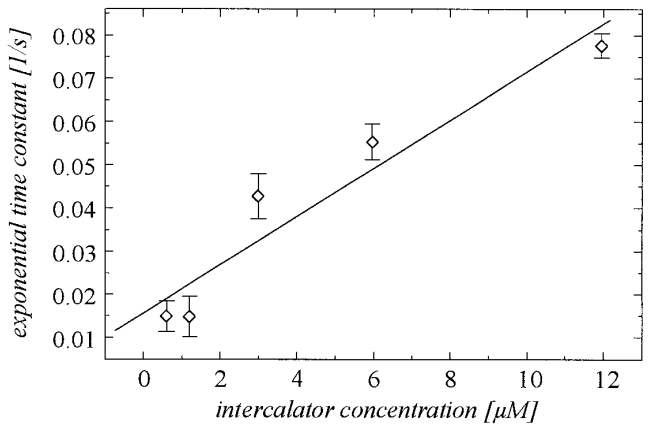

FIG. 10. Determination of the association rate from the exponential time constants k_s.

lution. During injection of the sample, several seconds are required to reach the actual sample concentration at the transducer surface. Within this period, interaction with the DNA occurs but the association kinetics is convoluted with an increase in concentration. Evaluation of the binding curve in this period requires deconvolution of these two functions and is therefore not practical. At high association rates, the entire binding occurs within this rise time and no accurate kinetic information is accessible from the binding curve.

The evaluation of the dissociation part of the binding curve by fitting an exponential decay is suitable for the investigation of the dissociation process in detail. Fitting of a single exponential function gave satisfying results only at low intercalator loadings and limited time periods of the dissociation part of the curve (Fig. 6). However, this behavior can also be ascribed to the different modes of interaction mentioned above. Furthermore, the probability of rebinding increases with decreasing occupation of the binding sites. For this reason the apparent dissociation rate constant will decrease with decreasing intercalator loading. A second exponential term was added to the model function to fit the curve in a more accurate manner. The dissociation rate constant of the faster dissociation process was used for the following evaluations and calculations.

For actinomycin D **(1)**, a dissociation rate constant k_d of 0.02 s^{-1} was determined from the fit which corresponds well to the dissociation rate constant determined from the exponential time constant of the association curve. For the other intercalators, dissociation rate constants up to 0.2 s^{-1} (for sanguinarine **(4)**) were found. Higher dissociation rate constants cannot be determined accurately by this method due to the sample handling because the same limitation applies to the washout and the dissociation as explained for the association kinetics.

The affinity constant of $3 \cdot 10^5$ liters/mol obtained from these rate constants for the intercalator actinomycin D **(1)** by using Eq. 2 corresponds well to the affinity constant determined from the equilibrium coverage. A comparison of all association and dissociation rate constants and the affinity calculated therefrom are summarized in Table 2. All affinity constants determined from binding kinetics are in good agreement with the results from the evaluation of the equilibrium coverage.

SUMMARY AND CONCLUSIONS

We have demonstrated label-free monitoring of specific binding of intercalators and other compounds to immobilized DNA using reflectometric interference spectroscopy. The binding effects observed by this technique were in good agreement with the melting curves for all compounds investigated. Surface coverages down to approximately 10 pg/mm^2 (i.e., approximately 5‰ with respect to the DNA loading) were detected unambiguously. Monitoring of the binding event at various intercalator concentrations allowed both a kinetic and thermodynamic characterization of the interaction with immobilized DNA. Intercalator binding was detectable down to concentrations of less than 0.1 μM. Affinity constants between $1 \cdot 10^5$ and $5 \cdot 10^6$ M^{-1} were derived from Scatchard plots of the equilibrium coverage and from the binding kinetics. These results are in accordance with the data found for these intercalators in literature. Two binding modes with different affinity constants and association rate constants were observed in agreement with results from homogeneous phase assays. Association rate constants in a range of 10^3–10^5 $M^{-1}s^{-1}$ and dissociation rate constants between $2 \cdot 10^{-1}$ and $2 \cdot 10^{-2}$ s^{-1} were observed.

For the detection of low-molecular-weight ligands, the number of binding sites at the surface is the limiting factor. Recently we have demonstrated that the detection of low-molecular-weight ligands binding to an immobilized receptor is feasible by RIfS down to a receptor concentration of approximately 10^{10} binding sites/mm^2 (35). Remarkably, the technique is not limited by the affinity constant of the interaction as far as the ligand concentration can be chosen high enough. The determination of rate constants is limited by the time resolution of the detection system and the sample handling system. Association rate constants between 10^3 and 10^5 liters/mol/s and dissociation rate constants between 10^{-1} and 10^{-4} s^{-1} can be determined by our present setup.

We have reported on a simple, rapid, and universal approach to study DNA–ligand interactions. The method described provides considerable potential for the investigation of low-molecular-weight ligands binding at DNA by biomolecular interaction analysis.

ACKNOWLEDGMENTS

We thank Professor Dr. A. Zeek for supplying us with decarestrictin D. Financial support by the BMBF (Biotechnology 2000, Project LIBRARIAN, Grant 0310838) is gratefully acknowledged. Corinna Maul was supported by a scholarship from the DECHEMA e. V.

REFERENCES

1. Wang, A. (1987) Interactions Between Antitumor Drugs and DNA, Nucleic Acids and Molecular Biology, Vol. 1, Springer-Verlag.
2. Waring, M. (1981) *Annu. Rev. Biochem.* **50,** 159–192.
3. Nováková, O., Vrána, O., Kiseleva, V., and Brabec, V. (1995) *Eur. J. Biochem.* **228,** 616–624.
4. Absalon, M., Kozarich, J., and Stubbe, J. (1995) *Biochemistry* **34,** 2065–2075.
5. Gao, X., Stassinopoulos, A., Rice, J., and Goldberg, I. (1995) *Biochemistry* **34,** 40–49.
6. Brown, J., and Imam, H. (1984) *Prog. Med. Chem.* **21,** 170–235.

7. Quillardet, P., Huisman, O., D'Ari, R., and Hofnung, M. (1982) *Proc. Natl. Acad. Sci. USA* **79,** 5971–5975.
8. Burres, N., Frigo, A., Rasmussen, R., and McAlpine, J. (1992) *J. Nat. Prod.* **55,** 1582–1587.
9. Pandey, P. C., and Weetall, H. H. (1995) *Anal. Chem.* **67,** 787–792.
10. Hotta, K., Zhu, C., Phomsuwansiri, P., Ishikawa, J., Mizuno, S., Hatsu, M., and Imai, S. (1995) *J. Antibiot.* **48,** 1267–1272.
11. Mahler, H., Goutarel, R., Khuong-Huu, Q., and Ho, M. (1966) *Nucleic Acid Int.* **5,** 2177–2191.
12. Karlsson, R. (1994) *Anal. Biochem.* **221,** 142–151.
13. Fägerstam, L. G., Frostell-Karlsson, A., Karlsson, R., Persson, B., and Rönnberg, I. (1992) *J. Chromatogr.* **597,** 397–410.
14. Liedberg, B., Nylander, C., and Lundström, I. (1983) *Sens. Act.* **4,** 299–304.
15. Cush, R., Cronin, J. M., Stewart, W. J., Maule, C. H., Molloy, J., and Goddard, N. J. (1993) *Biosens. Bioelectron.* **8,** 347–353.
16. Lukosz, W. (1995) *Sens. Act. B* **29,** 37–50.
17. Gauglitz, G., Brecht, A., Kraus, G., and Nahm, W. (1993) *Sens. Act. B* **11,** 21–27.
18. Karlsson, R. (1994) *Anal. Biochem.* **221,** 142–151.
19. Karlsson, R., and Stahlberg, R. (1995) *Anal. Biochem.* **228,** 274–280.
20. Piehler, J., Brecht, A., and Gauglitz, G. (1996) *Anal. Chem.* **68,** 139–143.
21. Langmuir, I., and Schaefer, V. J. (1937) *Science* **85,** 76–80.
22. Brecht, A., Gauglitz, G., and Polster, J. (1993) *Biosens. Bioelectron.* **8,** 387–392.
23. Brecht, A., and Abuknesha, R. (1997) In preparation.
24. Striebel, Ch., Brecht, A., and Gauglitz, G. (1994) *Biosens. Bioelectron.* **9,** 139–146.
25. Scatchard, G. (1949) *Ann. N. Y. Acad. Sci.* **51,** 660–672.
26. Karlsson, R., Michaelsson, A., and Mattson, L. (1991) *J. Immunol. Methods* **145,** 229–240.
27. O'Shannessy, D. J., Brigham-Burke, M., Soneson, K. K., Hensley, P., and Brooks, I. (1993) *Anal. Biochem.* **212,** 457–468.
28. Eddowes, M. J. (1987) *Biosensors* **3,** 1–15.
29. O'Shannessy, D. J., and Winzor, D. J. (1996) *Anal. Biochem.* **236,** 275–283.
30. Göhrt, A., Zeeck, A., Hütter, K., Kirsch, R., Kluge, H., and Thiericke, R. (1992) *J. Antibiot.* **45,** 66–73.
31. Reinhardt, C. G., and Krugh, T. R. (1978) *Biochemistry* **17,** 4845–4853.
32. Sinha, R. K., Talapatra, P., Mitra, A., and Mazumder, S. (1977) *Biochim. Biophys. Acta* **474,** 199–209.
33. Sen, A., and Maiti, M. (1994) *Biochem. Pharmacol.* **48,** 2097–2102.
34. Waring, M. J. (1970) *J. Mol. Biol.* **54,** 247–279.
35. Piehler, J., Maul, C., Brecht, A., Zerlin, M., Grabley, S., and Gauglitz, G. *Biosens. Bioelectron.*, in press.